Int J Thermophys (2016) 37:29
DOI 10.1007/s10765-016-2041-5

Co-registered Frequency-Domain Photoacoustic Radar and Ultrasound System for Subsurface Imaging in Turbid Media

Edem Dovlo[1] · **Bahman Lashkari**[1] · **Andreas Mandelis**[1]

Received: 6 October 2015 / Accepted: 18 January 2016 / Published online: 29 January 2016

Abstract Frequency-domain photoacoustic radar (FD-PAR) imaging of absorbers in turbid media and their comparison and/or validation as well as co-registration with their corresponding ultrasound (US) images are demonstrated in this paper. Also presented are the FD-PAR tomography and the effects of reducing the number of scan lines (or angles) on image quality, resolution, and contrast. The FD-PAR modality uses intensity-modulated (coded) continuous wave laser sources driven by frequency-swept (chirp) waveforms. The spatial cross-correlation function between the PA response and the reference signal used for laser source modulation produces the reconstructed image. Live animal testing is demonstrated, and images of comparable signal-to-noise ratio, contrast, and spatial resolution were obtained. Various image improvement techniques to further reduce absorber spread and artifacts in the images such as normalization, filtering, and amplification were also investigated. The co-registered image produced from the combined US and PA images provides more information than both images independently. The significance of this work lies in the fact that achieving PA imaging functionality on a commercial ultrasound instrument could accelerate its clinical acceptance and use. This work is aimed at functional PA imaging of small animals *in vivo*.

Keywords Biomedical imaging · Co-registration · Cross-correlation · Frequency-domain · Image improvement · Photoacoustic imaging · Ultrasound

✉ Andreas Mandelis
mandelis@mie.utoronto.ca

[1] Centre for Advanced Diffusion-Wave Technologies (CADIFT), Department of Mechanical and Industrial Engineering, University of Toronto, Toronto, ON M5S 3G8, Canada

1 Introduction

Cancer remains a major public health problem across the world, with a mortality rate of one in four deaths caused by cancer in the United States alone [1]. The chances of survival greatly increase when the disease is detected and treated at an earlier stage [2]. Photoacoustics technique, an emerging imaging modality based on the photoacoustic (PA) effect, is suitable for early breast cancer diagnosis [3,4], where, electromagnetic (EM) energy is absorbed to generate acoustic waves. PA imaging leverages the merits of optical and acoustic modalities by combining high optical contrast and spectroscopic-based specificity with high ultrasonic spatial resolution. PA imaging is sensitive to oxygenated hemoglobin concentration which is a critical diagnostic parameter for the metabolic state of lesions. Cancerous cells grow rapidly, thereby needing additional nutrients and oxygen, and thus, through the angiogenetic process, develop a dense microvasculature around themselves to perpetuate tumor growth. Through enhanced laser light absorption in the 650 nm to 1100 nm tissue optical spectral range, early cancer detection can be facilitated. Molecular and spectroscopic imaging is possible via applying multi-wavelength optical sources to the conventional PA modality [5–8].

1.1 Objective

Due to the strong induced signals and straightforward signal processing algorithms, most conventional PA imaging modalities have almost entirely employed pulsed laser PA with time-resolved measurements of acoustic transients for subsurface tumor detection [2,9]. As an alternative modality, frequency-domain photoacoustic radar (FD-PAR) imaging [10–13] uses compact, inexpensive continuous-wave (CW) laser diodes with a wide wavelength selection and has been shown to possess superior contrast [14] and depth-selective imaging capabilities [15]. It can generate high peak power cross-correlation responses through matched filtering. Signal-to-noise ratio (SNR) can also be significantly increased via pulse compression [16,17].

Moreover, combining PA imaging with other currently available detection modalities, including ultrasound (US) and optical methods, provides crucial complementary information through multifunction detection as a more accurate diagnostic tool. Human hand vasculature, sentinel lymph node detection, and cardiovascular dynamics in small animals have been reported in the literature using real-time US-*pulsed* PA systems [9,18]. Alternatively, we investigate the combination of our FD-PAR imaging system with US using a portable commercial US system (SonixTOUCH, Ultrasonix Medical Corp., Richmond, BC, Canada), especially simplified, since US imagers operate on frequency-domain principles and the same conventional US transducer array is employed for detection in both modalities, thereby accelerating the integration of the PAR accessory into the commercial US imager. Further image improvement techniques such as filtering, normalization, and amplification as well as tomography are explored in this study.

1.2 FD-PAR Theory

Our FD-PAR imaging system employs frequency-swept waveforms to drive the intensity-modulated (coded) CW laser source. A Fourier transform (FT) pair relates the frequency- and time-domain descriptions. Coherently averaging multiple chirps and maximizing the laser power, while staying below the maximum permissible exposure (MPE) by decreasing the chirp duration can further improve the system's SNR.

Subsurface absorbers (e.g., chromophores) absorb laser chirps (photons) when optically stimulated, resulting in the transmission of generated frequency-modulated acoustic waves propagating in the medium following thermoelastic energy conversion, which are far less-scattering (2–3 orders of magnitude weaker) than photons.

Under thermal confinement conditions, the excited pressure wave is governed by the inhomogeneous Helmholtz equation in the frequency domain (FD).

$$\left(\nabla^2 + k^2\right) \tilde{p}\left(\vec{r}, \omega\right) = -\frac{i\omega\beta}{C_p}\tilde{q}\left(\vec{r}, \omega\right) \tag{1}$$

where the tilde denotes the FT operation; β is the thermal expansion coefficient of the material; C_p is the specific heat capacity; $k = \omega/c_a$ is the acoustic wavenumber; $\omega = 2\pi f$ is the angular frequency; and $q\left(r, \omega\right)$ is the spectrum of the source term—the FT of the optical energy density per unit time at position, $\boldsymbol{r}$.

In the 1D model, the PA pressure detected at the transducer location ($z = -L$) using the laser-induced pressure transient generated at the absorber surface inside a turbid medium is given by

$$\tilde{p}_s\left(z = -L, f\right) = \frac{\Gamma_a}{\left(1 + \frac{\rho_a c_a}{\rho_s c_s}\right)} \frac{\mu_a}{\mu_a c_a + j\omega} e^{-jk_s L} \tilde{I}\left(f\right) \tag{2}$$

where $\Gamma_a = \beta_a c_a^2 / C_p$ is the Gruneisen coefficient (efficiency of thermoacoustic excitation); c_a is the speed of sound in the medium; $k_s = \omega/c_s$ is the wavenumber of the scattering medium; and $\tilde{I}\left(f\right)$ the optical intensity reaching the absorbing medium.

The cross-correlation of the PA response and the reference waveform used for laser source modulation are then used to determine the delay time needed for image reconstruction in the FD method.

2 Experimental Apparatus and Procedures

2.1 Co-registered FD-PAR and US *In Vivo* Animal Imaging

Figure 1 shows the experimental set-up. An 805-nm diode laser (Laser Light Solutions (LLS), NJ, USA) is employed to illuminate the sample at an output power of 6 W over a 2-cm beam diameter, i.e., ~1.91 W/cm^2 power density (less than half the calculated maximum permissible exposure (MPE) of 4.10 W/cm^2 for our CW system), and a standard commercial 64-element, 3.3-MHz phased array transducer (Ultrasonix Medical Corp., Richmond, BC, Canada) compatible with the Ultrasonix US imager is used

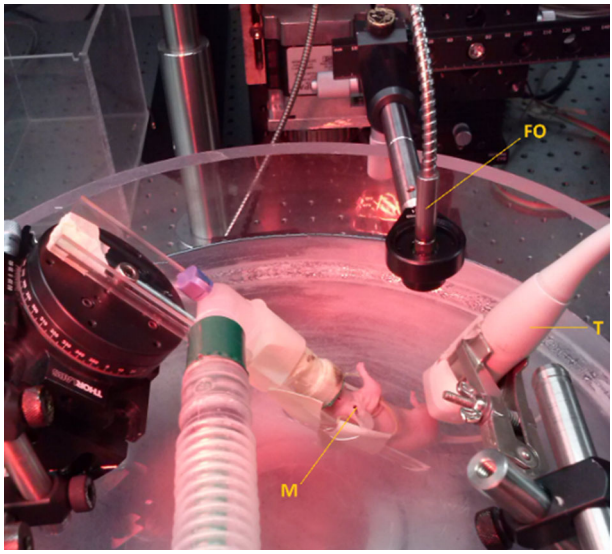

Fig. 1 Experimental set-up. *FO* fiber optic, *T* phased array transducer, *M* mouse

to detect the generated PA signals. Linear frequency-modulated (LFM) chirp signals (0.5 MHz–4 MHz, 1-ms duration) were generated for laser modulation using a signal-generation card. The sample and transducer surfaces were fully submerged in water to achieve acoustic coupling. Data acquisition and signal processing were performed using a data acquisition system and Lab View (National Instruments, Austin, TX, USA), as well as Matlab software (developed in-house). An economic and flexible synthetic receiver aperture and multiplexer system containing four programmable switch boards enable parallel readout of an 8-element subarray sequentially multiplexed over the entire array in reasonable time. Acquiring amplitude data takes ∼320 ms. System (hardware) modularity permits the subarray size and total number of channels to be increased for consecutive/ real-time imaging. A FD beam-forming algorithm was employed for the PA image reconstruction.

In order to perform *in vivo* animal testing, animal protocols were approved by the Division of Comparative Medicine (DCM) of the Faculty of Medicine, University of Toronto, and animal handling was performed according to the guide for animal care and laboratory use. A mouse was injected in its right thigh with cultured human hypopharyngeal head and neck squamous cell carcinoma FaDu cells. When a tumor became apparent, the experiment was performed with the animal fully anesthetized by applying 1.4 L/min of oxygen and 1 L/min of isofluorane gas, while its body temperature was kept constant using an IR lamp and a temperature controller.

The laser beam and transducer positioned in front of the thigh were moved together along the thigh to locate the tumor within. The generated PA image was optimized by adjusting the transducer once the tumor was located. Spatial registration of the two modalities was achieved by the use of the zero insertion force (ZIF) connector that fixed the transducer to the FD-PAR and Ultrasonix systems, allowing the PA and US

images to be produced at the same location with the US image providing structural guidance to the PA image.

2.2 FD-PAR Tomography

The FD-PAR tomography system employs a similar set-up to the one described above with a 3.5-MHz single-element transducer used for detection instead of the transducer array. The transducer can be revolved around the sample for data collection from multiple locations at multiple angles. Two graphite rods of different sizes (2 mm and 0.7 mm) arranged side-by-side were imaged using FD-PAR tomography. Various sampling step sizes were applied to explore the effect of reducing the number of scan lines on image quality, resolution and contrast.

3 Results

The SonixTOUCH US imager was used to obtain the pure US image of the cancer cell-injected mouse as shown in Fig. 2a. The tumor is difficult to distinguish among all the other body parts reflected such as bone, muscle, and fat (indicated by the dashed oval). The reconstructed PA images in Fig. 2, on the other hand, clearly indicate the

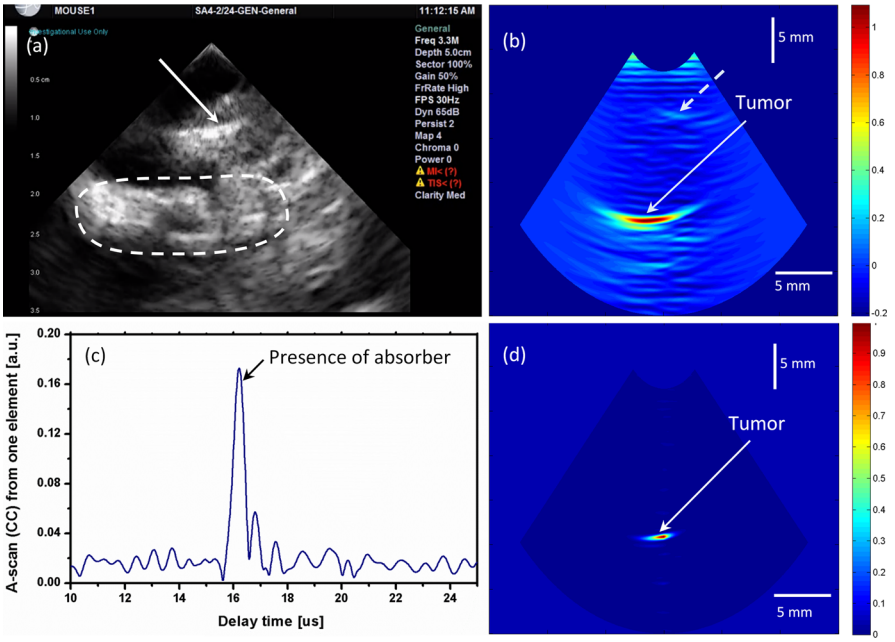

Fig. 2 (a) Pure US image showing the bottom edge of the plastic seat (*arrow*) and region of interest (*oval*); (b) Reconstructed PA image (exponential apodization); (c) Cross-correlation signal from one element of the transducer over the tumor location; (d) Improved post-amplification PA image of tumor in right thigh of nude mouse

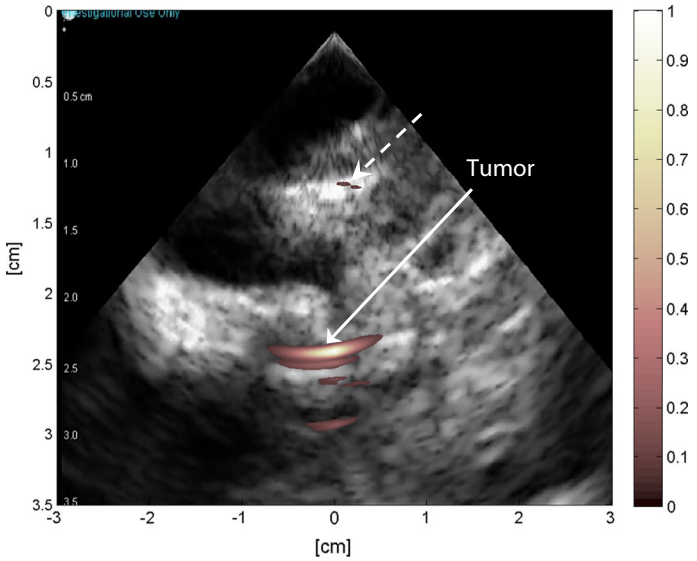

Fig. 3 Improved filtered PA image superimposed on the pure US image of the right thigh of the mouse

tumor located at ∼2.5 cm from the transducer surface, i.e., less than 3 mm below the skin. The PA image is highly sensitive to the presence of increased blood flow in the tumor, and is essentially much less sensitive to the presence of the surrounding body parts unlike the US image, thereby providing much clearer information regarding the tumor (i.e., better contrast and sensitivity). This leads us to hypothesize that the cancer may have increased the overall vascularity of the region of interest. The arrow in the US image matches the short-dashed arrow in the PA image, suspected to be the raised right foot of the mouse.

Various apodization functions and function combinations were tested. An exponential filter was applied in the PA image presented in Fig. 2b, with significant improvements observed in contrast and spatial resolution when the PA data were adequately normalized. Absorber spread and artifacts were further reduced by amplifying pixel intensities (Fig. 2d) where the image was first scaled to values within [0, 1] and then squared. It is important to note, however, that some relevant information could be lost or become difficult to identify afterward as seen from the loss of information (short-dashed arrows) in previous images, depending on how drastic the amplification is. Therefore, care must be taken in applying amplification. A cross-correlation signal (A-scan) corresponding to the amplitude PA images is shown in Fig. 2c, where the strong signal amplitudes (at ∼16-μs delay time) indicate the presence of the tumor. A scan of the mouse thigh further confirmed this by revealing similar increased signal strength at that same location when placed within the range of the transducer. The spatial extent of the tumor is represented in the images provided.

The co-registered image of the US and PA images is provided in Fig. 3. Tumor information obtained in the improved PA image is superimposed on the US image to provide enhanced tumor diagnostics, indicating the position of the tumor relative to the other body parts outlined in the US image as well as the spatial extent of the tumor.

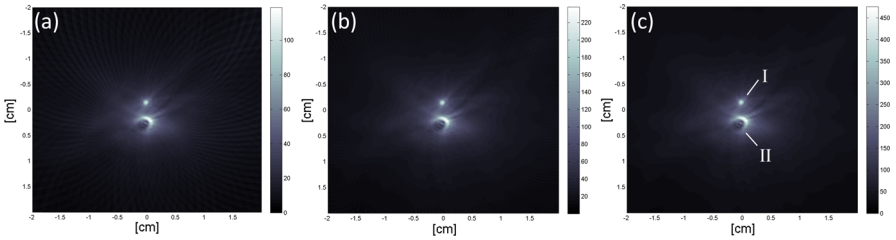

Fig. 4 Reconstructed tomographic images of two closely positioned graphite rods of different sizes obtained using (a) 91 (quarter) equally spaced scan lines, (b) 182 (half) equally spaced scan lines, and (c) 364 equally spaced scan lines, in one revolution

Figure 4 shows experimental results of the two graphite rods of different sizes (I—0.7-mm rod and II—2-mm rod) arranged side-by-side acquired by means of the FD-PAR tomography system. As observed in Fig. 4c, the larger diameter rod, II, is not illuminated internally as the PA signal originates in regions close to the surface of the rod. Optical intensity is significantly reduced beyond the surface due to strong absorption at the surface. The image, although obtained without filtering, normalization, or amplification as done in the aforementioned single-location FD-PAR imaging, shows good quality and spatial resolution. Interference patterns are observed to increase as the number of scan lines decreases. However, the system still produces adequate results even when as few as one-quarter of the number of the original scan lines in a complete revolution ($\sim 1^\circ$ step-size) are used.

4 Conclusion

A co-registered US and FD-PAR image is reported in this paper. It explores capitalizing on the strengths of both modalities for accurate tumor localization and detection. Filtering methods as well as image normalization and amplification techniques were applied to improve FD-PAR imaging parameters such as SNR, contrast, and spatial resolution. A cancer cell-injected mouse was imaged to illustrate co-registration and image improvement. FD-PAR tomography was also demonstrated, providing images of high quality and improved spatial resolution. Adequate image quality was still achievable with a quarter of the original number of scan lines used. Further studies are underway to fully amalgamate both modalities into a single portable clinical imager.

Acknowledgments AM is grateful to the Natural Sciences and Engineering Research Council of Canada (NSERC) for a Discovery Grant and to Samsung Advanced Institute of Technology (SAIT) through a Global Research Outreach (GRO) Research Project Grant.

References

1. R. Siegel, J. Ma, Z. Zou, A. Jemal, CA Cancer J. Clin. **64**, 1 (2014)
2. M. Xu, L.V. Wang, Rev. Sci. Instrum. **77**, 4 (2006)
3. S. Mallidi, G.P. Luke, S. Emelianov, Trends Biotechnol. **29**, 5 (2011)
4. L.V. Wang, H. Wu, *Biomedical Optics: Principles and Imaging* (Wiley, Hoboken, 2012)

5. J.-T. Oh, M.-L. Li, H.F. Zhang, K. Maslov, G. Stoica, L.V. Wang, J. Biomed. Opt. **11**, 3 (2006)
6. D. Razansky, M. Distel, C. Vinegoni, R. Ma, N. Perrimon, R.W. Köster, V. Ntziachristos, Nat. Photonics **3**, 7 (2009)
7. S. Telenkov, A. Mandelis, Rev. Sci. Instrum. **81**, 12 (2010)
8. B. Lashkari, S. Soo Choi, E. Dovlo, S. Dhody, A. Mandelis, IEEE J. Sel. Top. Quantum Electron. 99 (2015)
9. P. Beard, Interface Focus **1**, 4 (2011)
10. S. Telenkov, A. Mandelis, B. Lashkari, M. Forcht, J. Appl. Phys. **105**, 10 (2009)
11. S. Telenkov, A. Mandelis, J. Biomed. Opt. **14**, 4 (2009)
12. S. Kellnberger, N.C. Deliolanis, D. Queirós, G. Sergiadis, V. Ntziachristos, Opt. Lett. **37**, 16 (2012)
13. P. Mohajerani, S. Kellnberger, V. Ntziachristos, Opt. Lett. **39**, 18 (2014)
14. B. Lashkari, A. Mandelis, Rev. Sci. Instrum. **82**, 9 (2011)
15. S. Telenkov, A. Mandelis, J. Biomed. Opt. **11**, 4 (2006)
16. S.A. Telenkov, R. Alwi, A. Mandelis, W. Shi, E. Chen, A.I. Vitkin, in SPIE BiOS, p. 82231J (2012)
17. E. Dovlo, B. Lashkari, A. Mandelis, W. Shi, F.-F. Liu, Biomed. Opt. Express **6**, 3 (2015)
18. S. Telenkov, R. Alwi, A. Mandelis, A. Worthington, Opt. Lett. **36**, 23 (2011)